Spatial variability of quickflow and its determinants in Tamaulipas, México from the InVEST seasonal water yield model

Mariela Estefanía Nava-Vélez[1, *], Kyle Blount[2], Glenda Nelly Requena-Lara[1], René Ventura-Houle[1] and Juan Francisco Morales Pacheco[1]

[1]Faculty of Engineering and Sciences, Autonomous University of Tamaulipas, Ciudad Victoria, Tamaulipas, Mexico; nava.velez.mariela@gmail.com; grequena@uat.edu.mx; rventura@docentes.uat.edu.mx

[2]School of Integrated Sciences, Sustainability and Public Health, University of Illinois Springfield, Springfield, Illinois, USA; wblou2@uis.edu

Keywords: Quickflow, InVEST, LULC, Soil, Runoff, Precipitation.

Abstract

Quickflow (QF) is the fraction of rainfall that rapidly runs off to channels, a key element for understanding floods and designing control measures. It reflects rapid runoff pathways that drive peak flows, sediment pulses, water-quality downstream impacts, and hazards. QF is influenced by the precipitation regime (seasonality and event concentration) and by surface properties represented by land use/land cover (LULC) and soil types, which modulate infiltration and storage. We applied the InVEST–Seasonal Water Yield (SWY) model at 30 m resolution in the San Fernando–Soto la Marina basin. We used monthly climate, 2020 LULC, and soil type data, and analyzed (i) the basin-wide distribution of QF, (ii) the spatial influence of LULC- and soil-based on QF, and (iii) the precipitation–QF relationship. Results show a multimodal distribution of QF ratios; urban areas, bare soils, and low-cover croplands yield higher QF than woody covers; and the precipitation–QF relationship is positive but dispersed, modulated by the sequence and intensity of events and by surface conditions. We conclude that integrated land and water management should (a) focus on targeted interventions in high-QF zones that maintain or improve vegetation cover and promote infiltration to reduce flooding and erosion and promote increased dry season flows and (b) integrate improved temporal and spatial representation of precipitation events with realistic LULC and soil parameterizations for more accurate model outputs and reliable planning.

1. Introduction

The study of QF is an essential component of hydrological analysis, as it helps elucidate the processes that govern the movement of water over the Earth's surface and its relationship with the physical and environmental characteristics of a watershed (Reitz, 2019). The QF parameter represents the fraction of precipitation that flows directly to channels without infiltrating into the soil, making it a key indicator of surface hydrological behavior and the immediate response of a basin to rainfall events (Yamasaki et al., 2023).

In Tamaulipas, México, the importance of characterizing quick runoff is reflected in the historical disaster pattern: between 1999 and 2018, storms and tropical cyclones accounted for the largest share of FONDEN (Natural Disasters Fund) resources allocated to the state (1.79 billion and 0.93 billion MXN, respectively), far exceeding other disaster types such as fluvial, pluvial, or drought events. Moreover, storm declarations have shown the highest frequency and municipal coverage, with notable peaks such as 2013 (99 municipalities affected) (INECC, 2021; DOF, 2013). This pattern indicates high exposure to intense rainfall and rapid hydrological responses, so quantifying and mapping quickflow is especially relevant for risk management and water-resource planning in the state (INECC, 2021).

Understanding the spatial and temporal dynamics of runoff is crucial, since excessive quickflow can generate significant hydrological and environmental consequences, such as flooding, soil erosion, loss of fertility, transport of sediments and pollutants, and reduced aquifer recharge (Kayitesi et al., 2022; Tedoldi et al., 2016). These impacts affect not only ecosystems but also human activities, infrastructure, and the water security of communities (Amundson et al., 2015; Mishra et al., 2021; Othman et al., 2023). Therefore, detailed analysis of this phenomenon is essential for sustainable water management and land-use planning (Haasnot et al., 2011; Russo et al., 2014).

Multiple physical and environmental factors control the generation and magnitude of quickflow on the landscape (Lang et al., 2025). Chief among them is precipitation, which determines the amount of water available for infiltration and overland flow (Kirkby et al., 1969; Orchard et al., 2012). Topography directly influences the velocity of surface flow and the land's capacity to retain or infiltrate water (Price et al., 2011; Anderson and Burt, 1978). Soil properties and type, in turn, determine infiltration, permeability, and storage characteristics, which directly affect the proportion of runoff generated (Hümann, et al., 2011; Yand and Zhang, 2011). Land use and land cover also play a decisive role, as impervious or degraded surfaces tend to increase volumes of surface runoff (Zimmermann et al., 2006; Dias et al., 2015).

Recent research has demonstrated that spatiotemporal characterization of land-use and land-cover dynamics using high-resolution remote sensing and machine-learning tools can substantially improve the detection of patterns relevant to hydrological processes, particularly in urban or environmentally stressed basins (Rodríguez González et al., 2024). Such LULC-oriented approaches provide valuable support for runoff-related assessments by refining the representation of surface conditions that control infiltration and rapid flow responses.

A widely used parameter to integrate the influence of these factors is the Curve Number (CN), developed by the USDA Soil Conservation Service (SCS). This index synthesizes a surface's hydrological response by combining soil type, land cover, management practices, and antecedent moisture conditions,

This contribution has been peer-reviewed. The double-blind peer-review was conducted on the basis of the full paper.
https://doi.org/10.5194/isprs-annals-X-3-W3-2025-69-2026

becoming a fundamental tool for estimating surface runoff in hydrological models (Brandão et al., 2025; Wang et al., 2025).

In this context, spatial modeling tools such as the InVEST (Integrated Valuation of Ecosystem Services and Tradeoffs) model are highly useful for comprehensively evaluating quickflow and partitioning of the hydrologic cycle (Raji et al., 2021). The InVEST Seasonal Water Yield (SWY) model estimates the generation and spatial distribution of runoff from climatic, topographic, edaphic, and land-cover information, enabling the identification of areas with greater susceptibility to runoff and associated processes (Hamel et al., 2020). Its application strengthens understanding of hydrological processes and informs management and conservation strategies in watersheds (Wang et al., 2016).

This study evaluates the spatial variability of quickflow (QF) using InVEST by (1) describing its basin-wide distribution, (2) comparing QF across LULC classes and soil types while accounting for their areal shares, and (3) assessing the relationship between annual precipitation and QF across the study area.

2. Study Area

San Fernando–Soto la Marina basin is located between 25°44′02.49″ N - 23°16′55.93″ N and 98°47′23″ W - 98°24′21.10″ W, in the state of Tamaulipas (Figure 1). Its terrain ranges from coastal plains and rolling hills to the ranges of the Sierra Madre Oriental, which lie to the west of the area (DOF, 2018).

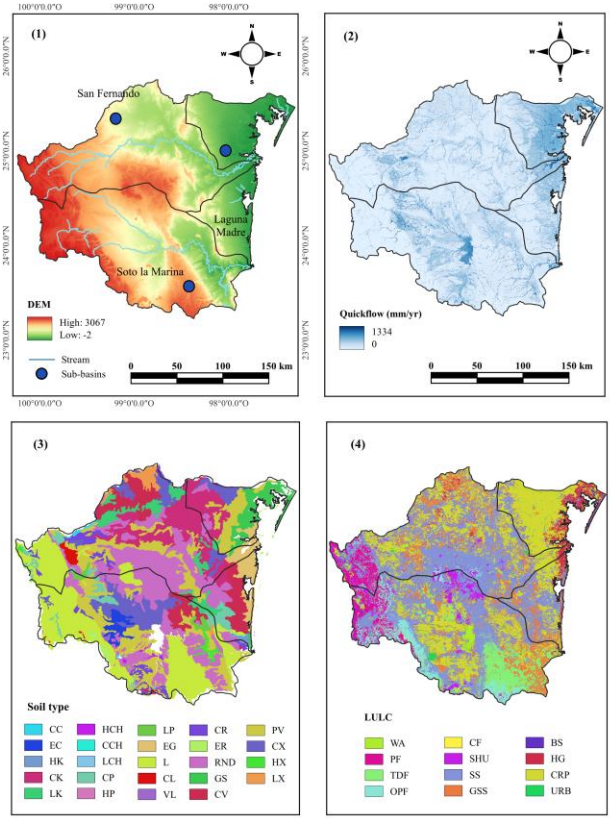

Figure 1. San Fernando-Soto la Marina basin in Tamaulipas, México, showing (1) study site, (2) quickflow, (3) soil type; categorized as calcaric cambisol (CC), eutric cambisol (EC), haplic kastanozem (HK), calcaric kastanozem (CK), luvic kastanozem (LK), haplic chernozem (HCH), calcaric chernozem (CCH), luvic chernozem (LCH), calcaric phaeozem (CP), haplic phaeozem (HP), luvic phaeozem (LP), eutric gleysol (EG), leptosol (L), chromic luvisol (CL), vertic luvisol (VL), calcaric regosol (CR), eutric regosol (ER), rendzina (RND), gleyic solonchak (GS), chromic vertisol (CV), pelic vertisol (PV), calcaric xerosol (CX), haplic xerosol (HX), luvic xerosol (LX) and (4) land use/land cover (LULC); categorized as water (WA), pine forest (PF), tropical dry forest (TDF), oak-pine forest (OPF), cloud forest (CF), shrubland (SHU), submontane shrublands (SS), grassland (GSS), bare soil (BS), halophytic grassline (HG), cropland (CRL) and urban zone (URB).

Tamaulipas experiences its highest average maximum temperatures in June and August (34.6 °C and 34.5 °C), while the lowest values occur in December and January (11.2 °C and 10.6 °C) (INECC, 2021). Precipitation (P) is greatest during the June–October wet season, reaching a maximum in September (160.4 mm). These seasonal patterns frame a heterogeneous land-use/land-cover (LULC) mosaic set over diverse soils across the state (INEGI, 2014; CONABIO, 2023).

3. Data and Methods

3.1 InVEST model

The InVEST SWY is a simple, spatially explicit hydrologic model that estimates the seasonal contribution of the landscape to runoff (Natural Capital Project, 2025). It operates at a monthly scale using climate, LULC, and soils to partition the hydrologic response into quickflow (rapid runoff) and slower components (i.e., recharge and baseflow) (Guswa et al., 2018). Its outputs are relative indices, useful for comparing scenarios and seasons; the quick-flow equation is presented below (eq. 1). This flow is computed using a CN based method, assuming that daily rainfall depths on rainy days follow an exponential distribution (Natural Capital Project, 2025). Its outputs are relative indices, useful for comparing scenarios and seasons; the quick-flow equation is presented below:

$$QF_{i,m} = n_m \times \left((a_{i,m} - S_i) exp\left(-\frac{0.25_i}{a_{i,m}}\right) + \frac{S_i^2}{a_{i,m}} exp\left(\frac{0.85_i}{a_{i,m}}\right) E_1\left(\frac{S_i}{a_{i,m}}\right) \right) \times \left(25.4\left[\frac{mm}{in}\right]\right), \quad (1)$$

where n_m = number of rainfall events at pixel i during month m

$a_{i,m}$= mean rainfall depth on a rainy day at pixel i during month m

$S_i = \frac{1000}{CN_i} - 10$; CN_i= curve number for pixel i

E_1 = exponential integral function

QF_i the annual quickflow, is computed as the sum of the monthly values $QF_{i,m}$

3.2 InVEST model inputs

A 30 m DEM (USGS/NASA, 2024) was used for topography; 2020 LULC (CONABIO–CONAFOR–INEGI, 2020; Landsat-8, 30 m) for land cover/use; and the Soil Map, Series II (INEGI, 2014) for soil types (Figure 1). Soil polygons were reclassified into USDA Hydrologic Soil Groups (A–D) using INEGI descriptions of the soil classes, and Curve Number (CN) values

This contribution has been peer-reviewed. The double-blind peer-review was conducted on the basis of the full paper.
https://doi.org/10.5194/isprs-annals-X-3-W3-2025-69-2026 | © Author(s) 2026. CC BY 4.0 License.

were assigned by combining LULC and soil groups using the USDA SCS lookup table, ensuring unique runoff responses for each pairing. Climate inputs included monthly precipitation from CRU-TS v4.09 downscaled with WorldClim 2.1 (Harris et al., 2020; Fick & Hijmans, 2017) and potential evapotranspiration from the CGIAR-CSI Global PET dataset (Trabucco & Zomer, 2019). As these rasters represent monthly totals, no temporal aggregation was needed; all inputs were clipped to the basin and linked through monthly CSV tables.

Long-term rainfall event normals (e.g., the number of events per month from January through December) from SMN meteorological stations were spatially interpolated using the Inverse Distance Weighting (IDW) method to create continuous climate-zone maps differentiated by mean monthly precipitation events. Based on these, a rainfall-events table was generated to indicate the number of rainy days (> 0.1 mm) per month. The InVEST SWY model uses the CSV rainfall events table to partition total monthly precipitation into discrete storm events and the GeoTIFF climate-zone raster to assign each pixel to a representative climatic regime, enabling simulation of spatially variable quickflow (Natural Capital Project, 2025).
A biophysical table linked each LULC class to hydrologic parameters, incorporating vegetation coefficients (Kc) from FAO guidelines (Allen et al., 1998) and Curve Number (CN) ranges recommended by the USDA-NRCS (1986) and the InVEST User Guide (Natural Capital Project, 2025) (Figure 2).

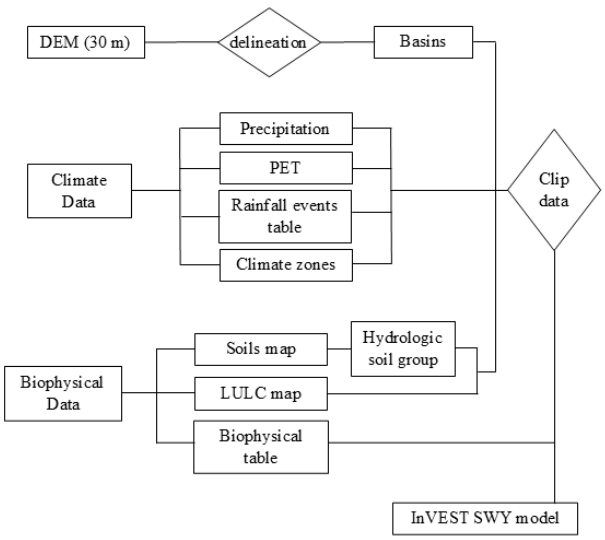

Figure 2. A schematic illustration of the Seasonal Water Yield (SWY) model workflow for quickflow estimation.

4. Results

4.1 Pixel-scale distribution of QF/P across the basin

The distribution of QF/P is right-skewed and multimodal (Figures 1(2) and 2). Three well-defined peaks are observed at 0–0.12 (n = 620,478), 0.22–0.30 (n = 225,070), and 0.48–0.56 (n = 108,499). The mass of the distribution is concentrated below 0.20, followed by a mid-range peak and a smaller high-value peak (Figure 2).

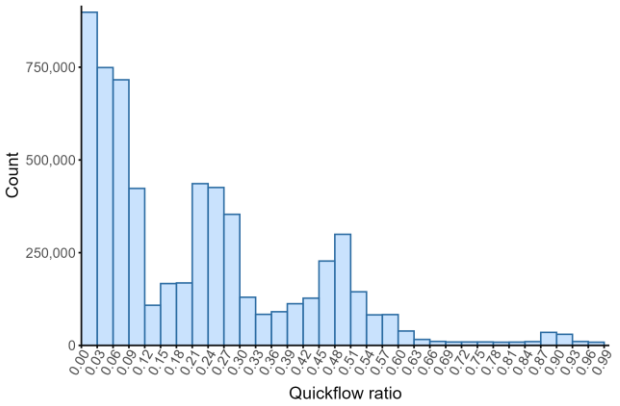

Figure 3. Histogram of the quickflow ratio (QF/P).

4.2 Quickflow variability across LULC and soil types

QF differed markedly among LULC classes (Figure 3). The highest median QF was observed in water (WA; 870.8 mm/yr). An intermediate group included Halophytic grassline (HG;530.1 mm/yr), Urban zone (URB; 395.2 mm/yr), Cropland (CRL; 384.5 mm/yr), and Bare soil (BS; 363.8 mm/yr). Lower medians were observed for Shrubland (SHU; 171.0), Grassland (GSS; 137.2 mm/yr), and Tropical dry forest (TDF; 117.2 mm/yr), whereas Submontane shrublands (SS;63.5 mm/yr) and Cloud forest (CF;41.5 mm/yr) were very low, and Pine forest (PF; 3.6 mm/yr) and Oak-pine forest (OPF; 1.8 mm/yr) clustered near 0 mm/yr. All classes included observations of 0 mm/yr QF.

Areal proportions provide critical context: despite high medians, water (WA), Halophytic grassline (HG), Urban zone (URB), and Bare soil (BS) occupy only 1.07%, 1.71%, 0.60%, and 0.86% of the basin, respectively (Table 1), while Submontane shrubland (SS) (20.79%) and Cropland (CRL) (16.81%) dominate the landscape, followed by Grassland (GSS) (6.63%), Tropical dry forest (TDF) (3.32%), Oak-pine forest (OPF) (2.90%), Pine forest (PF) (2.67%), and Shrubland (SHU) (1.90%). Thus, basin-wide QF patterns are shaped by high-QF but spatially limited classes and by extensive low-to-moderate classes with large area shares.

QF varied markedly across soil types (Figure 4). Median QF spanned 0.51–610.27 mm/yr, with the highest medians in Gleyic Solonchak (GS; 610.27 mm/yr), Eutric Gleysol (EG; 514.59 mm/yr), and Pelic Vertisol (PV; 417.13 mm/yr). A mid-range was observed for Luvic Phaeozhem (LP; 345.63 mm/yr), Calcaric Xerosol (CX; 316.33 mm/yr), Vertic Luvisol (VL; 277.01 mm/yr), Eutric Cambisol (EC; 270.58 mm/yr), Haplic Xerosol (HX; 253.28 mm/yr), Chromic Luvisol (CL; 252.74 mm/yr), and Chromic Vertisol (CV; 250.53 mm/yr). Lower medians occurred in (RND; 69.24 mm/yr), Luvic Kastanozem (LK; 70.88 mm/yr), Luvic Chernozem (LCH; 71.71 mm/yr), Calcaric Phaeozem (CP; 76.81 mm/yr), Calcaric Kastanozem (CK; 87.99 mm/yr), Calcaric Regosol (CR; 96.69 mm/yr), Calcaric Chernozem (CCH; 114.22 mm/yr), Calcaric Cambisol (CC; 119.58 mm/yr), Luvic Xerosol (LX; 171.24 mm/yr), Haplic Chernozem (HCH; 198.55 mm/yr), and Haplic Phaeozem (HP; 204.97 mm/yr), with LIT (33.74 mm/yr) and Eutric Regosol (ER; 0.51 mm/yr) at the bottom. Most soil types include 0 mm/yr observations; Luvic Phaeozem (LP), Vertic Luvisol (VL), Eutric Cambisol (EC), and Luvic Chernozem (LCH) do not. Several violins display elongated upper tails, indicating a strong right-skew.

This contribution has been peer-reviewed. The double-blind peer-review was conducted on the basis of the full paper.
https://doi.org/10.5194/isprs-annals-X-3-W3-2025-69-2026 | © Author(s) 2026. CC BY 4.0 License.

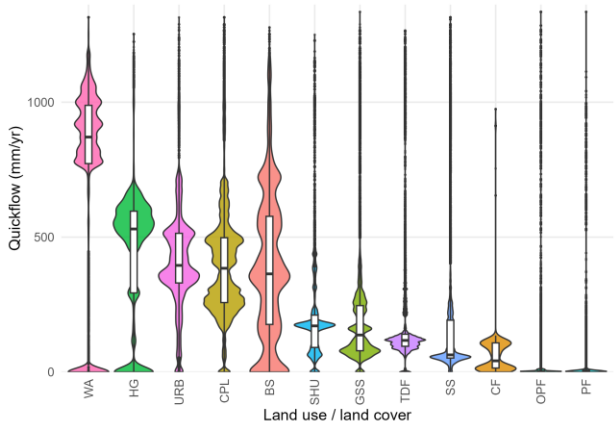

Figure 4. Violin/boxplots of QF (mm/yr) by LULC; classes ordered by median; boxes display median and IQR.

Table 1. Areal extent of LULC (km²; % of basin).

LULC	Area (km²)	%
SS	17155.12	20.79
CRL	13876.73	16.81
GSS	5468.92	6.63
TDF	2736.95	3.32
OPF	2391.03	2.90
PF	2202.71	2.67
SHU	1569.53	1.90
HG	1409.65	1.71
WA	884.52	1.07
BS	709.94	0.86
URB	493.72	0.60
CF	13.88	0.02

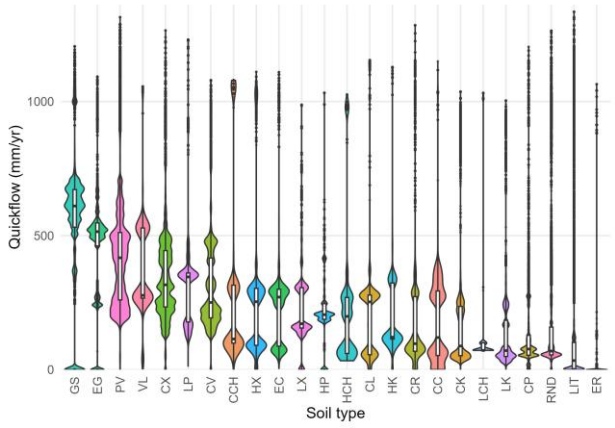

Figure 5. Violin/boxplots of QF (mm/yr) by soil type; types ordered by median; boxes show median and IQR.

Areal composition provides essential context (Table 2): three classes dominate the basin: RND (9,603.99 km²; 20.37%), LIT (8,674.84 km²; 18.40%), and PV (7,200.82 km²; 15.27%) together accounting for 54% of the area. Mid-extent classes include CK (9.88%), CX (7.69%), and CV (7.50%), followed by LK (3.47%), GS (3.19%), EG (3.07%), CP (2.81%), and CR (2.44%). Smaller fractions correspond to LX (1.39%) and EC (1.26%), whereas the remaining soil types each occupy <1% of the basin, the smallest being LCH, 0.01%. Thus, basin-wide QF patterns reflect the interplay between a few high-QF soils with modest areal contributions and extensive low-to-moderate QF soils that dominate the landscape.

Table 2. Area and percentage by soil type class in the San Fernando-Soto la Marina basin

Soil	Area (km²)	%
RND	9603.99	20.37
LIT	8674.84	18.40
PV	7200.82	15.27
CK	4657.78	9.88
CX	3625.26	7.69
CV	3535.23	7.50
LK	1634.93	3.47
GS	1501.74	3.19
EG	1445.38	3.07
CP	1322.72	2.81
CR	1151.98	2.44
LX	657.00	1.39
EC	593.50	1.26
LP	355.90	0.75
HX	294.45	0.62
CL	270.76	0.57
ER	191.77	0.41
CC	102.80	0.22
HK	98.59	0.21
HCH	70.35	0.15
HP	68.12	0.14
VL	54.77	0.12
CCH	27.07	0.06
LCH	2.85	0.01

4.3 Precipitation–quickflow relationship

The P-QF relationship is positive, with the upper envelope of quickflow increasing as precipitation rises. The fitted linear model (R^2 = 0.21) summarizes this basin-wide association and indicates a moderate relationship with substantial dispersion around the trend (Figure 6). This dispersion reflects the wide range of QF values observed across the basin for similar precipitation levels. At the monthly scale, the relationship varied considerably, with very low coefficients of determination ($R^2 \leq 0.02$) in most months and a modest peak during July (R^2 = 0.13), indicating that the strength of the P–QF association changes seasonally but is strongest at the annual scale.

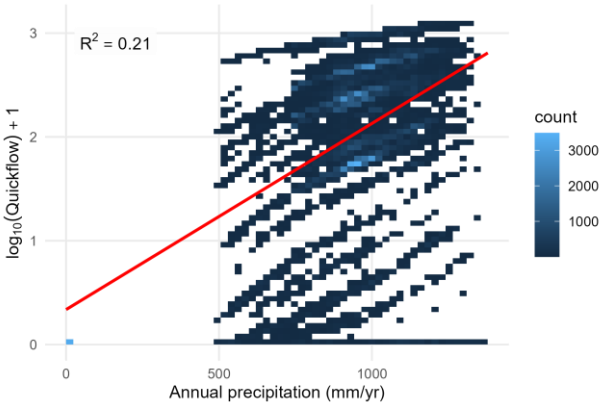

Figure 6. Relationship between annual precipitation and log(QF)+1; density shading indicates observation counts. The fitted trend is positive (R^2 = 0.21).

5. Discussion

5.1 Distribution of quickflow ratios

The multimodal distribution of QF/P, skewed to the right, indicates that most pixels contribute little to direct runoff in an average year, while a smaller group clusters around

This contribution has been peer-reviewed. The double-blind peer-review was conducted on the basis of the full paper.
https://doi.org/10.5194/isprs-annals-X-3-W3-2025-69-2026 | © Author(s) 2026. CC BY 4.0 License.

intermediate and high fractions. This pattern is consistent with a landscape where (i) precipitation is seasonally concentrated and spatially uneven (Good et al., 2016), (ii) infiltration capacity varies considerably with soil structure and vegetation (Jencso et al., 2011), and (iii) hydrological connectivity differs among terrain units.

Areas with dense tree cover, higher infiltration capacity, or longer overland flow paths tend to populate the low QF/P mode, while zones with shallow or poorly structured soils, sparse vegetation, or short and well-connected flow paths between hillslopes and channels tend to occupy the higher modes (Kumar et al., 2021). Pixels with QF values close to zero likely reflect locations where vegetation and soils prevent most rainfall from becoming QF (Hamel et al., 2020).

These characteristics align with the CN-based representation of quickflow in SWY, where antecedent moisture, soil group, and LULC jointly modulate the distribution of a given rainfall depth (Muche et al., 2020). In summary, multimodality is to be expected in a watershed that combines coastal lowlands, agricultural plains, shrublands, and forested highlands.

Importantly, the distribution pattern of intermediate-to-high QF/P fractions (Figure 6) identifies areas where rapid hydrological response could amplify the impacts of intense or atypical rainfall events. High-fraction pixels may coincide with sectors that are more prone to rapid accumulation and runoff concentration during storms, especially in landscapes where drainage density or flow-path connectivity is high (Hamel et al., 2020; Xu et al., 2020). These spatial signals align with the disaster patterns described for Tamaulipas and point to potential subareas where hydrometeorological vulnerability is elevated.

5.2 LULC and soil impacts on QF

Classes associated with low infiltration or effective imperviousness (e.g., Urban zone [URB], Bare soils [BS], Croplands [CRL], Halophytic grassline [HG]) typically show higher QF values than forest covers (Xu et al., 2020; Zhang et al., 2017). However, their basin-scale influence depends on the areal extent of each LULC class: several high-QF classes may occupy small fractions (e.g., Water [WA], Halophytic grassline [HG], Urban zone [URB], and Bare soil [BS]), whereas extensive classes with moderate or low QF (e.g., Submontane shrublands [SS], Cropland [CRL], Grasslands [GSS], and Tropical dry forests [TDF]) determine the aggregated signal (Zhang et al., 2017; Xu et al., 2020). From a mechanistic perspective, vegetation structure, rooting depth, and surface roughness attenuate event responses in forests and some shrublands, whereas sparse canopies, soil disturbance, or imperviousness amplify them in urban, agricultural, or bare settings (Zhang et al., 2017; Li et al., 2017).

Soils indicative of low permeability, shallow profiles, salinity/alkalinity issues, or shrink–swell behavior (e.g., Gleyic Solonchak [GS], Eutric Gleysol [EG], and Pelic Vertisol [PV]) tend to exhibit higher QF medians and longer upper tails; in contrast, deeper soils with better structure or coarser texture (e.g., Eutric Regosol [ER], Litosol [LIT], Calcaric Regosol [CR], Calcaric Cambisol [CC], Calcaric Chernozem [CCH], Luvic Kastanozem [LK], and Luvic Chernozem [LCH]) show lower medians (Issa et al., 2011; Mandal et al., 2008; Bagarello et al., 2014).
As with LULC, area matters: some high-QF soils do not dominate basin-wide responses if they are distributed in isolated patches, whereas more widespread low- to moderate-QF soils govern the basin's aggregated values (Zhang et al., 2017).
These gradients align with long-standing evidence that land cover and soil hydraulic properties co-control runoff generation via infiltration-excess and saturation-excess processes urbanization and ground exposure increase quickflow, while forested or undisturbed covers reduce it (Stewart et al., 2019; Xu et al., 2020; Zhang et al., 2017) and the CN-based parameterization used by the SWY model intentionally integrates LULC and soil information; therefore, the observed ranges are consistent with CN theory (Natural Capital Project, 2025; USDA-NRCS, 1986; Guswa et al., 2018).

The spatial arrangement of these LULC–soil combinations also highlight areas that may be more vulnerable to hydrometeorological hazards. High-QF classes concentrated near drainage lines, lowlands, or urbanized sectors can accelerate surface runoff during intense storms, increasing susceptibility to localized flooding. Conversely, forested and well-vegetated zones function as hydrological buffers, suggesting priority areas for conservation or restoration to mitigate the impacts of extreme rainfall (Zhang et al., 2017; Xu et al., 2020). These spatial contrasts underscore how QF maps can support the identification of critical subareas relevant for disaster prevention and risk-reduction planning.

5.3 Evaluation of precipitation – quickflow relationship

At the basin scale, we observe a positive QF-P trend: more precipitation generally produces more quickflow. However, the weak fit ($R^2 = 0.21$) and the large spread around the trend indicate that QF is shaped not only by rainfall totals but also by the temporal structure of rainfall and the surface conditions controlling the partitioning between runoff and infiltration. Within the InVEST–SWY framework, which implements a CN-based formulation, this behavior is expected because the model responds to the depth of rainfall on rainy days and the number of effective events, rather than to monthly or annual precipitation alone (Natural Capital Project, 2025; USDA NRCS, 1986).

A key factor behind this dispersion is event sequencing. Months with the same total rainfall can generate markedly different QF depending on whether precipitation occurs as many small storms or as a few large storms. This pattern is also supported by the weak relationships between precipitation and quickflow in individual months ($R^2 < 0.02$ for all months except July). Fewer, more intense events produce higher mean storm depths and therefore greater QF, whereas numerous small events often generate lower QF, even under similar precipitation totals. Similarly, antecedent soil moisture modulates the runoff response between successive storms. Temporal clusters of rainfall events limit drying time and increase antecedent soil moisture, reducing infiltration and amplifying QF; in contrast, widely spaced storms allow drying and increased infiltration capacity, yielding lower QF. These mechanisms help explain why pixels subjected to similar precipitation exhibit contrasting QF values and why the relationship follows an envelope pattern rather than a tight linear trend (Hamel et al., 2020).

Previous applications of InVEST–SWY report similar outcomes: precipitation is the primary driver of QF, but land cover, soil hydrologic group, event frequency, and storm intensity jointly determine how closely QF follows rainfall at fine spatial scales (Natural Capital Project, 2025; Hamel et al., 2020). Improving representations of event sequencing,

vegetation dynamics, and soil moisture states has been shown to strengthen the precipitation–runoff relationship.

In practice, relying on annual precipitation alone can underestimate QF in urban or compacted areas where antecedent moisture and storm clustering greatly increase runoff and overestimate QF in vegetated or highly permeable areas, where infiltration dominates (Ran et al., 2022; O'Driscoll et al., 2010). Therefore, planning and assessment should integrate precipitation scenarios with realistic LULC and soil parameterizations and, when possible, incorporate information on the temporal distribution and sequencing of rainfall events, particularly in urbanizing basins where increases in runoff are well documented (Chen et al., 2017; Huang et al., 2024).

5.4 Study Limitations and Model Constraints

Like other InVEST tools, the SWY model provides a simplified representation of hydrological processes and is primarily designed for comparative or scenario-based analyses. QF estimation relies on the CN approach, which simplifies the surface-runoff relationship and does not explicitly incorporate topographic variability or event-scale dynamics. Consequently, the model does not effectively capture short-term fluctuations associated with extreme precipitation events or the non-linear response of saturated areas (Natural Capital Project, 2025).

Temporal resolution represents another key limitation. The SWY model operates at a monthly time step, which smooths peak flows and prevents accurate reproduction of event-based runoff or flood magnitudes. Thus, the outputs are best interpreted as relative indicators of spatial variation rather than absolute discharge values. This temporal aggregation also affects the representation of antecedent moisture and storm sequencing, which influence quickflow generation in real-world conditions.

Uncertainties may also arise from the parameterization of input datasets. The CN and Kc values are assigned by land-cover class and soil hydrologic group, assuming homogeneity within each class. These empirical values are based on generalized tables and may not reflect local soil structure, vegetation condition, or management practices. Similarly, rainfall and evapotranspiration inputs derived from global datasets (e.g., WorldClim, CGIAR-CSI) involve downscaling and interpolation steps that introduce additional spatial uncertainty.

Finally, the SWY framework uses simplified flow routing and does not simulate groundwater-surface water interactions, channel transmission losses, or feedbacks between land cover and evapotranspiration. As a result, the model's outputs are more reliable for identifying spatial patterns and relative differences in QF across the basin than for quantifying absolute magnitudes. While effective as a tool to inform long-term water resource management through spatial patterns and trends in water yield across years to decades, these limitations necessitate caution when applying SWY model results to questions the model is not designed to answer.

6. Conclusions

Taken together, these results meet the study's objective by: (1) describing a multimodal QF distribution, (2) identifying systematic contrasts by LULC and soil while accounting for area, and (3) confirming a primary precipitation control tempered by surface properties.

(1) In the San Fernando–Soto la Marina basin, quickflow (QF) is highly heterogeneous: most areas contribute little in a typical year, while a smaller area shows intermediate to high values, consistent with the combined effects of seasonal precipitation, land cover/use, and soil properties. (2) For LULC, urban zones, bare soils, and crops with low cover tend to generate more QF than woody covers; however, at the basin scale, most of the land area contributes very little, whereas high-QF zones, especially where flow paths are short, contribute most of the QF.

For soils, those associated with waterlogging/salinity and shrink–swell clays (e.g., GS, EG, PV) tend to generate higher QF than deeper, better-structured, or coarser soils (e.g., ER, LIT, CR, CC, CCH, LK, LCH); however, at the basin scale, the overall behavior is determined by the extensive low-to-moderate QF soils, while the high-QF classes being more limited in area have less influence on the total outcome. (3) The precipitation–QF relationship is positive but weak: annual rainfall totals alone are not good predictors of local QF because the sequence/intensity of events and surface conditions modulate runoff generation within the InVEST–SWY framework (CN-based).

These results bear important implications for improving watershed and water resource management. For instance, regional management should focus on combining targeted actions in zones that are prone to waterlogging and rapid runoff improving retention and reducing quickflow to prevent flooding and erosion (e.g., urban drainage upgrades and protection of exposed or agricultural soils) with broader actions across the rest of the basin to maintain vegetation and enhance water infiltration. Future work should integrate precipitation scenarios with realistic LULC and soil parameterizations and, when possible, evaluate the impact of seasonal and event-specific differentiation of precipitation, to avoid under- or overestimating QF.

Acknowledgements

This work was supported by the Secretaría de Ciencia, Humanidades, Tecnología e Innovación (SECIHTI) through a doctoral scholarship (No. 4014305), and by the Autonomous University of Tamaulipas (UAT) through a mobility grant.

Rferences

Amundson, R., Berhe, A.A., Hopmans, J.W., Olson, C., Sztein, A.E., Sparks, D.L., 2015. Soil and human security in the 21st century. *Science*, 348(6235), 1261071. doi.org/10.1126/science.1261071

Allen, R.G., Pereira, L.S., Raes, D., Smith, M., 1998. Crop Evapotranspiration – Guidelines for Computing Crop Water Requirements (FAO Irrigation and Drainage Paper No. 56). *Food and Agriculture Organization of the United Nations*, Rome.

Anderson, M.G., Burt, T.P., 1978. The role of topography in controlling throughflow generation. *Earth Surf. Process*. Landf., 3(4), 331–344. doi.org/10.1002/esp.3290030402

Bagarello, V., Castellini, M., Di Prima, S., Iovino, M., 2014. Soil hydraulic properties determined by infiltration experiments and different heights of water pouring. *Geoderma* 213, 492–501. doi.org/10.1016/j.geoderma.2013.08.032

Brandão, A.R.A., Schwamback, D., Ballarin, A.S., Ramirez-Avila, J.J., Oliveira, P.T.S., 2025. Toward a better understanding of curve number and initial abstraction ratio values from a large sample of watersheds perspective. *J. Hydrol.*, 655, 132941. doi.org/10.1016/j.jhydrol.2025.132941

Chen, J., Theller, L., Gitau, M.W., Engel, B.A., Harbor, J.M., 2017. Urbanization impacts on surface runoff of the contiguous United States. *J. Environ. Manage*. 187, 470–481. doi.org/10.1016/j.jenvman.2016.11.017

CONABIO, 2023. Nuevo mapa de la cobertura de suelo de México. Gobierno de México – Comisión Nacional para el Conocimiento y Uso de la Biodiversidad (CONABIO). gob.mx/conabio/prensa/nuevo-mapa-de-la-cobertura-de-suelo-de-mexico (30 September 2025).

Dias, L.C.P., Macedo, M.N., Costa, M.H., Coe, M.T., Neill, C., 2015. Effects of land cover change on evapotranspiration and streamflow of small catchments in the Upper Xingu River Basin, Central Brazil. *J. Hydrol.: Reg. Stud*., 4, 108–122. doi.org/10.1016/j.ejrh.2015.05.010

DOF, 2013: Declaratoria de Desastre Natural por tormenta tropical (19–22 junio 2013), Estado de Tamaulipas. Diario Oficial de la Federación, 3 de julio de 2013.

DOF, 2018. Acuerdo por el que se dan a conocer los resultados del estudio técnico y se establecen reservas de aguas nacionales superficiales en la Región Hidrológica No. 25 San Fernando–Soto la Marina. Diario Oficial de la Federación. dof.gob.mx (30 April 2025).

Fick, S.E., Hijmans, R.J., 2017. WorldClim 2.1: new 1-km spatial resolution climate surfaces for global land areas. *International Journal of Climatology*, 37(12), 4302–4315. doi.org/10.1002/joc.5086

Good, S.P., Guan, K., Caylor, K.K., 2016. Global Patterns of the Contributions of Storm Frequency, Intensity, and Seasonality to Interannual Variability of Precipitation. *Journal of Climate* 29(1). doi.org/10.1175/JCLI-D-14-00653.1

Guswa, A.J., Hamel, P., Meyer, K., 2018. Curve Number approach to estimate monthly and annual direct runoff. *Journal of Hydrologic Engineering,* 23(2). doi.org/10.1061/(ASCE)HE.1943-5584.0001606.

Haasnoot, M., Middelkoop, H., van Beek, E., van Deursen, W.P.A., 2011. A Method to Develop Sustainable Water Management Strategies for an Uncertain Future. *Sust. Dev*. 19(6), 369–381. doi.org/10.1002/sd.438

Hamel, P., Valencia, J., Schmitt, R., Shrestha, M., Piman, T., Sharp, R.P., Francesconi, W., Guswa, A.J., 2020. Modeling seasonal water yield for landscape management: Applications in Peru and Myanmar. *J. Environ. Manage*., 270, 110792. doi.org/10.1016/j.jenvman.2020.110792

Harris, I., Osborn, T.J., Jones, P.D., Lister, D.H., 2020. Version 4 of the CRU TS monthly high-resolution gridded multivariate climate dataset (CRU-TS v4.09). Scientific Data, 7, 109. doi.org/10.1038/s41597-020-0453-3

Huang, S., Gan, Y., Chen, N., Wang, C., Zhang, X., Li, C., Horton, D.E., 2024. Urbanization enhances channel and surface runoff: A quantitative analysis using both physical and empirical models over the Yangtze River basin. *J. Hydrol*. 635, 131194. doi.org/10.1016/j.jhydrol.2024.131194

Hümann, M., Schüler, G., Müller, C., Schneider, R., Johst, M., Caspari, T., 2011. Identification of runoff processes – The impact of different forest types and soil properties on runoff formation and floods. *J. Hydrol*., 409, 637–649. doi.org/10.1016/j.jhydrol.2011.08.067

INECC, 2021. Tamaulipas — Vulnerabilidad. Portal Estados y Municipios, Instituto Nacional de Ecología y Cambio Climático. cambioclimatico.gob.mx/estadosymunicipios/Vulnerabilidad/V_28.html (19 September 2025).

INEGI, 2014. Conjunto de Datos Vectorial Edafológico, escala 1:250 000 (Serie II). Instituto Nacional de Estadística y Geografía. inegi.org.mx (1 October 2025).

Issa, O., Valentin, C., Rajot, J.L., Cerdan, O., Desprats, J.-F., Bouchet, T., 2011. Runoff generation fostered by physical and biological crusts in semi-arid sandy soils. *Geoderma* 167–168, 22–29. doi.org/10.1016/j.geoderma.2011.09.013

Jencso, K.G., McGlynn, B.L., 2011. Hierarchical controls on runoff generation: Topographically driven hydrologic connectivity, geology, and vegetation. *Water Resources Research* 47, W11527. doi.org/10.1029/2011WR010666

Kayitesi, N.M., Guzha, A.C., Mariethoz, G., 2022. Impacts of land use land cover change and climate change on river hydro-morphology—A review of research studies in tropical regions. *J. Hydrol*., 615, 128702. doi.org/10.1016/j.jhydrol.2022.128702

Kirkby, M.J., 2020. Infiltration, Throughflow and Overland Flow. En: Introduction to Fluvial Geomorphology (ed. M.J. Kirkby), Routledge, London, pp. 68–102.

Kumar, A., Kanga, S., Taloor, A.K., Singh, S.K., Đurin, B., 2021. Surface runoff estimation of Sind River Basin using integrated SCS-CN and GIS techniques. *HydroResearch* 4, 61–74. doi.org/10.1016/j.hydres.2021.08.001

Lan, J., Wang, H., Su, Y., Huang, L., Guo, W., 2025. Linking quickflow and circuit theory to identify potential flood diffusion corridors and their interregional transmission mechanisms. *Environment, Development and Sustainability.* doi.org/10.1007/s10668-025-06439-2

Li, Q., Wei, X., Zhang, M., Liu, W., Fan, H., Zhou, G., Giles-Hansen, K., Liu, S., Wang, Y., 2017. Forest cover change and water yield in large forested watersheds: A global synthetic assessment. *Ecohydrology* 10, e1838. doi.org/10.1002/eco.1838

Mandal, U.K., Bhardwaj, A.K., Warrington, D.N., Goldstein, D., Bar-Tal, A., Levy, G.J., 2008. Changes in soil hydraulic conductivity, runoff, and soil loss due to irrigation with different types of saline–sodic water. *Geoderma* 144(3-4), 509-516. doi.org/10.1016/j.geoderma.2008.01.005

Mishra, B.K., Kumar, P., Saraswat, C., Chakraborty, S., Gautam, A., 2021. Water Security in a Changing Environment: Concept, Challenges and Solutions. *Water*, 13(4), 490. doi.org/10.3390/w13040490

Muche, M.E., Hutchinson, S.L., Hutchinson, J.M.S., Johnston, J.M., 2019. Phenology-adjusted dynamic curve number for

improved hydrologic modeling. *Journal of Environmental Management* 235, 403–413. https://doi.org/10.1016/j.jenvman.2018.12.115

USGS/NASA, 2024. NASADEM Merged DEM Global 1 arc second V001 [data set]. NASA EOSDIS Land Processes DAAC.

Natural Capital Project, 2025. Seasonal Water Yield — InVEST User Guide (Build 3.17). Stanford University. storage.googleapis.com/releases.naturalcapitalproject.org/invest-userguide/latest/en/seasonal_water_yield.html (20 March 2025).

Orchard, C., Lorentz, S.A., Jewitt, G.P.W., Chaplot, V., 2013. Spatial and temporal variations of overland flow during rainfall events and in relation to catchment conditions. *Hydrological Processes,* 27(16), 2325–2338. doi.org/ 10.1002/hyp.9217

Othman, A., El-Saoud, W.A., Habeebullah, T., Shaaban, F., Abotalib, A.Z., 2023. Risk assessment of flash flood and soil erosion impacts on electrical infrastructures in overcrowded mountainous urban areas under climate change. *Reliab. Eng. Syst. Saf.* 236, 109302. doi.org/10.1016/j.ress.2023.109302

Price, K., 2011. Effects of watershed topography, soils, land use, and climate on baseflow hydrology in humid regions: A review. *Progress in Physical Geography* 35(4), 465–492. doi.org/0.1177/0309133311402714

O'Driscoll, M., Clinton, S., Jefferson, A., Manda, A., McMillan, S., 2010. Urbanization effects on watershed hydrology and in-stream processes in the southern United States. *Water* 2(3), 605–648. doi.org/10.3390/w2030605

Ran, Q., Wang, J., Chen, X., Liu, L., Li, J., Ye, S., 2022. The relative importance of antecedent soil moisture and precipitation in flood generation in the middle and lower Yangtze River Basin. *Hydrology and Earth System Sciences* 26, 4919–4931. doi.org/10.5194/hess-26-4919-2022

Raji, S.A., Odunuga, S., Fasona, M., 2021. Spatial Appraisal of Seasonal Water Yield of the Sokoto-Rima Basin. Sakarya *University Journal of Science*, 25(4), 950–968. doi.org/10.16984/saufenbilder.800302

Reitz, M., Sanford, W.E., 2019. Estimating quick-flow runoff at the monthly timescale for the conterminous United States. *Journal of Hydrology* 573, 841–854. doi.org/10.1016/j.jhydrol.2019.04.010

Rodríguez González, K. D., Arista Cázares, L. E., and Yépez Rincón, F. D., 2024. Spatiotemporal land use land cover (LULC) change analysis of urban narrow river using Google Earth Engine and Machine learning algorithms in Monterrey, Mexico, *ISPRS Ann. Photogramm. Remote Sens. Spatial Inf.* Sci., X-3-2024, 371–375, doi.org/10.5194/isprs-annals-X-3-2024-371-2024

Russo, T., Alfredo, K., Fisher, J., 2014. Sustainable Water Management in Urban, Agricultural, and Natural Systems. *Water* 6, 3934–3956. doi.org/10.3390/w6123934

Servicio Meteorológico Nacional (SMN), Comisión Nacional del Agua (CONAGUA), 2025: Normales climatológicas por estado. Disponible en: https://smn.conagua.gob.mx/es/climatologia/informacion-climatologica/normales-climatologicas-por-estado

Stewart, R.D., Bhaskar, A.S., Parolari, A.J., Herrmann, D.L., Jian, J., Schifman, L.A., Shuster, W.D., 2019: An analytical approach to ascertain saturation-excess versus infiltration-excess overland flow in urban and reference landscapes. *Hydrological Processes* 33(26), 3349–3363. doi.org/ 10.1002/hyp.13562.

Tedoldi, D., Chebbo, G., Pierlot, D., Kovacs, Y., Gromaire, M.-C., 2016. Impact of runoff infiltration on contaminant accumulation and transport in the soil/filter media of Sustainable Urban Drainage Systems: A literature review. *Sci. Total Environ.,* 569–570, 904–926. doi.org/10.1016/j.scitotenv.2016.04.215

Trabucco, A., Zomer, R.J., 2019. Global Aridity Index (Global-Aridity) and Potential Evapotranspiration (Global-PET) Climate Database v2. CGIAR-CSI (Consortium for Spatial Information). doi.org/10.6084/m9.figshare.7504448.v3

USDA Soil Conservation Service (SCS), 1986. Urban Hydrology for Small Watersheds (TR-55), 2nd ed., Conservation Engineering Division, Washington, DC. (Appendix A updated January 1999).

Wang, G., Mang, S., Cai, H., Liu, S., Zhang, Z., Wang, L., Innes, J.L., 2016. Integrated watershed management: evolution, development and emerging trends. *Journal of Forestry Research* 27(5), 967–994. doi.org/ 10.1007/s11676-016-0293-3

Wang, M., Zhao, Y., Shi, W., Yu, J., Chen, T., Bao, J., Song, W., Chen, H., 2025: A modified curve number method for runoff prediction of different soil types in China. *CATENA* 254, 108957. doi.org/10.1016/j.catena.2025.108957

Xu, C., Rahman, M., Haase, D., Wu, Y., Su, M., Pauleit, S., 2020. Surface runoff in urban areas: The role of residential cover and urban growth form. *J. Clean. Prod*. 262, 121421. doi.org/10.1016/j.jclepro.2020.121421

Yamasaki, T., Hamamoto, S., Nishimura, T., 2023. Base flow separation for soil erosion simulation in a granitic forested headwater catchment using a process-based model, GeoWEPP. Int. *J. Sediment Res.*, 38(4), 494–502. doi.org/10.1016/j.ijsrc.2023.04.003

Yang, J.-L., Zhang, G.-L., 2011. Water infiltration in urban soils and its effects on the quantity and quality of runoff. *Journal of Soils and Sediments* 11, 751–761. doi.org/ 10.1007/s11368-011-0356-1

Zhang, M., Liu, N., Harper, R., Li, Q., Liu, K., Wei, X., Ning, D., Hou, Y., Liu, S., 2017. A global review on hydrological responses to forest change across multiple spatial scales: Importance of scale, climate, forest type and hydrological regime. *Journal of Hydrology* 546, 44–59. doi.org/10.1016/j.jhydrol.2016.12.040

Zimmermann, B., Elsenbeer, H., De Moraes, J.M., 2006. The influence of land-use changes on soil hydraulic properties: Implications for runoff generation. *For. Ecol. Manage*. 222, 29–38. doi.org/:10.1016/j.foreco.2005.10.070